Heavy-ion fusion cross section formula and barrier height distribution

C. L. Jiang* and B. P. Kay
Physics Division, Argonne National Laboratory, Argonne, Illinois 60439, USA

(Received 14 April 2022; accepted 23 May 2022; published 3 June 2022)

Methods for obtaining fusion cross section formulas are discussed, especially for those that take on an empirical form. A new expression starting with $\sigma(E) = \frac{1}{E}\int_{E_0}^{E}(\int_{E_0}^{E'} B(E'')dE'')dE'$ has been explored. Here, $B(E)$ is a reasonable, assumed function of the barrier height distribution, $\frac{d^2(\sigma E)}{dE^2}$. The resulting analytic cross section formula reproduces very well the excitation functions for many light and heavy fusion systems across wide energy ranges, when $B(E)$ is assumed to be a multi-Gaussian function. This study offers an improved determination of the fusion barrier height distribution over other numerical techniques.

DOI: 10.1103/PhysRevC.105.064601

I. INTRODUCTION

Heavy-ion fusion reactions, arguably the most complex process in the interaction between two atomic nuclei, have been investigated extensively for sixty years. More than one thousand excitation functions have already been measured and collected in the literature [1]. Some recent articles have reviewed these studies in detail [2–7].

The study of the interplay between the reaction dynamics and nuclear structure, the synthesis of very heavy elements, and the extension of the nuclear chart towards the neutron-rich side and neutron-deficient side of β stability constitute various struggling efforts. However, attempts to obtain fusion cross-section formulas remain central to theoretical studies from the beginning until the present day.

The excitation function, $\sigma(E)$, is most commonly depicted either in linear or logarithmic scales. However, because of the steepness of the excitation function at near- or sub-barrier energies, it is difficult to recognize possible structures as well as deviations from theoretical curves, especially in logarithmic plots. In order to alleviate this problem, one often uses other representations of $\sigma(E)$ in the comparison of measurements and theoretical calculations, e.g., as reviewed in Ref. [7]. A particular representation may emphasize the behavior of the excitation function in some part of the energy range and specific structure local to this energy range. In principle, any theoretical calculation which can reproduce the experimental excitation function must also reproduce all the other representations as well.

In this article, two related issues are presented. First, the two commonly used methods developed to obtain fusion cross section formulas are summarized. We then explore a third, new method, the *reciprocal of a fusion representation*, from which a fusion cross section formula has been obtained. This new formula reproduces a large number of excitation functions for light and heavy fusion systems across wide energy region exceptionally well.

Second, because this fusion cross section formula and the corresponding barrier height distribution $B(E) = \frac{d^2(\sigma E)}{dE^2}$ are all analytic, the "ambiguity" problem in previous studies of barrier height distributions has been avoided, and thus accurate barrier-height spectra can be obtained.

II. DIFFERENT METHODS FOR CALCULATING FUSION CROSS SECTIONS

A. Fundamental method

Starting from the equation of the two colliding nuclei, assuming the interaction between them, combining the nuclear structure input, etc., one derives a fusion cross section formula, $\sigma(E)$. The classical, strong absorption model [8],

$$\begin{aligned}\sigma(E) &= \pi R^2(1 - B/E) \quad \text{for } E > B,\\ &= 0 \quad \text{for } E < B,\end{aligned} \tag{1}$$

and the Wong formula [9],

$$\sigma_w(E) = \frac{R^2\hbar\omega}{2E}\ln\left[1 + \exp\left(2\pi\frac{E - V}{\hbar\omega}\right)\right]. \tag{2}$$

are well known examples. Here, R and V are the barrier radius and barrier height, and ω in Eq. (2) is the frequency of the inverted harmonic potential.

The above method is the fundamental one for obtaining the fusion cross sections, since it is based on the essential physics ingredients, although some approximations are often involved. Coupled channels (CC) calculations and many other theoretical approaches by using Schrödinger or other equations belong to this category also, although they result in numerical calculations and not analytic formulas (see Refs. [10,11] and [2–7]).

*jiang@phy.anl.gov

B. Modifications from previous cross section formulas

Stelson developed another method to calculate the fusion excitation function. He was the first to introduce the expression

$$\sigma(E) = \int \sigma(E, B)D(B)dB \tag{3}$$

to fit the experimental fusion excitation function [12]. Here, $\sigma(E, B)$ is a *known* (previously obtained) excitation function with a single barrier with a height B. Importantly, he assumed that there are more than one barrier with different heights during the collision of the two nuclei, and introduced the distribution of barrier heights $D(B)$. The function, $D(B)$, contains adjustable parameters which are determined in the fitting process comparing with the experimental data. In general, $\sigma(E, B)$ in Eq. (3) can be either an analytic function or even a known dataset of an experimental excitation function or calculation results.

Rowley *et al.* [13] found that the experimental barrier height distribution $D(E)$ can be extracted from a precise experiment of the fusion excitation function via the second derivative:

$$D(E) = \frac{1}{\pi R^2}\frac{d^2(\sigma(E)E)}{dE^2}, \quad \text{with} \int D(E)dE = 1. \tag{4}$$

After that, many studies have concentrated on obtaining the barrier height distribution and the understanding of the corresponding reaction dynamics by comparing the experimental barrier distributions in Eq. (4) with the results of CC calculations. Then, the double-differentiation process is used to obtain the barrier distribution both for experiments and calculations.

In Refs. [14,15], Siwek-Wilczyńska *et al.* applied Stelson's idea mentioned above to calculate the fusion cross sections. They started from an expression based on the blackbody approximation [8] and assumed that the barrier height distribution, $D_g(B)$, is a Gaussian function:

$$\sigma(E)E = \pi R^2 \int_{E_0}^{E} (E - B)D_g(B)dB, \tag{5}$$

$$D_g(B) = \frac{1}{\sqrt{2\pi}W}\exp\left[-\left(\frac{B - V}{\sqrt{2}W}\right)^2\right]. \tag{6}$$

The resulting analytic cross section formula is

$$\sigma(E)E = \pi R_0^2 \frac{W}{\sqrt{2\pi}}[\sqrt{\pi}Z\,\mathrm{erfc}(-Z) + \exp(-Z^2)], \tag{7}$$

with $Z = (E - V)/\sqrt{2}W$, where V and W are the centroid and the standard deviation of the Gaussian function.

This formula given by Eq. (7) was developed in their studies exploring the production of superheavy elements, and the comparisons of this formula with the experimental data were mostly in the cross section range of about 0.1–1000 mb. This method has not been widely used and referenced in the literature.

At around the same time, the heavy-ion fusion hindrance phenomenon at extreme sub-barrier energies was discovered [16–18], which is concerned with fusion dynamics at low cross section, typically less than 0.1 mb. Just recently, Jiang *et al.* [19], found that the fusion formula of Siwek-Wilczyńska *et al.*, Eq. (7), can reproduce the fusion hindrance behavior very well, including the S-factor maximum. In Ref. [19], a table was included which analyzed 29 fusion systems whose excitation function has been measured down to lower than 0.01 mb.[1]

There are many ways to modify fusion cross-section formulas by making modifications to known formulas. Two recent examples, Refs. [22] and [23], made modifications to the Wong formula [9] and achieved much better results than the original.

C. A reciprocal of a fusion representation

In this paper we demonstrate that there is a third kind of method to obtain the fusion cross section formula, namely, by using a *reciprocal* of a fusion representation. This method has been used implicitly before, but has never been illustrated as a method in the literature.

It is well known that a straightforward signature of the heavy-ion fusion hindrance behavior is the appearance of a maximum of the astrophysical $S(E)$ factor at low energies [17,18]. This is a significant structure seen in $S(E)$ but not in $\sigma(E)$. At the same time, in another representation, the logarithmic derivative,

$$L(E) = \frac{d[\ln(\sigma E)]}{dE}, \tag{8}$$

the slope of $L(E)$ as a function of E, gets steeper and steeper with decreasing energy. In Refs. [24,25], empirical recipes to describe the behavior of $L(E)$ at low energies and to extrapolate the excitation function to even lower energy were formulated, via a two-parameter expression:

$$L(E) = A_0 + \frac{B_0}{(E + Q_0)^{3/2}}. \tag{9}$$

Q_0 is either 0 or the fusion Q value depending on whether the fusion Q value is either positive or negative, respectively. Parameters A_0 and B_0 are obtained from least-squares fits to the experimental $L(E)$ data at low energies. From Eq. (9), the corresponding cross section formula was derived in Refs. [24] and [25]:

$$\sigma(E) = \sigma_s \frac{E_s}{E}\exp\Bigg(A_0(E - E_s) - \frac{2B_0}{\sqrt{E_s + Q_0}}\left[\sqrt{\frac{E_s + Q_0}{E + Q_0}} - 1\right]\Bigg). \tag{10}$$

E_s is the energy at the S-factor maximum, determined from parameters A_0 and B_0 with the equation

$$L(E_s) = L_{cs}(E_s) = \frac{\pi\eta}{E_s^{3/2}}. \tag{11}$$

[1]The hindrance phenomenon was explained first by Mişicu and Esbensen [20] by considering the saturation properties of nuclear matter, and later by Ichikawa *et al.* [21], among others, with various models. In this paper we do not discuss the theoretical explanation of the fusion excitation function.

Here, $L_{cs}(E)$ is the constant S-faction function [17], η is the Sommerfeld parameter $Z_1Z_2e^2/(\hbar v)$, and v is the relative velocity of the two heavy ions.

It is important to note that Eq. (10) was obtained with the reciprocal of the representation $L(E) = \frac{d[\ln(\sigma E)]}{dE}$, namely

$$\sigma(E) = \frac{1}{E}\exp\left[\int_{Q_0}^{E}(L_{\text{test}}(E'))dE'\right]a, \tag{12}$$

without any approximation. Here, $L(E)$ in Eq. (12) is written as $L_{\text{test}}(E)$ and taken as Eq. (9).

In fact, any reasonable analytic function $L_{\text{test}}(E)$ with adjustable parameters, not necessarily Eq. (9), can be applied in Eq. (12), and leads to a cross section formula. By comparing the calculated results with the experimental fusion excitation function and using the least-squares fitting technique, the optimum parameters in $L_{\text{test}}(E)$ can be determined. For example, one may assume an $L_{\text{test}}(E)$ other than Eq. (9), which can describe not only the $\sigma(E)$ at low energies but also at the high energy range. It is outside the scope of the present article and will be studied in the future.

Now we explore a new heavy-ion fusion cross section expression. By applying the *reciprocal* on another fusion representation,

$$B_{\text{test}}(E) = \frac{d^2(\sigma E)}{dE^2} = \pi R_0^2 D_{\text{test}}(E),$$
$$\text{with} \int D_{\text{test}}(E)dE = t1, \tag{13}$$

one obtains a new cross section formula:

$$\sigma(E)E = \int_{E_0}^{E}\left(\int_{E_0}^{E'}\frac{d^2(\sigma E'')}{d(E'')^2}dE''\right)dE'$$
$$= \pi R_0^2\int_{E_0}^{E}\left(\int_{E_0}^{E'}D_{\text{test}}(E'')dE''\right)dE'. \tag{14}$$

Here, R_0 is a normalization constant for the function $D_{\text{test}}(E)$. The lower integration limits in Eq. (14) are $E_0 = -Q$ or 0, depending on whether the fusion Q value is negative or positive, respectively.

Any reasonable analytic function $D_{\text{test}}(E)$ with adjustable parameters can be used in Eq. (14). By comparing the results with the experimental fusion excitation function using least-squares fitting techniques, the optimum parameters for the assumed $D_{\text{test}}(E)$ function will be determined.

When Rowley *et al.* derived Eq. (4), approximations were introduced: the classical expression of fusion cross section for a barrier of radius R was used, together with the assumption that the radius R is independent of the the barrier height $B(E)$. While Eq. (13) is similar to Eq. (4), it is defined without any approximations, and is thus an exact formula. All approximations are contained in the assumption of function $B_{\text{test}}(E)$. It should be mentioned that the upper limit of Eq. (13) should not be infinity, but a finite number. In the study of low energy nuclear physics, one always restricts the discussion within a certain energy range, since other degrees of freedom may appear outside the energy limit. In practice, the values of $D_{\text{test}}(E)$ at an energy near the high energy limit are often negligible.

After testing a variety of barrier distributions we found that a sum of L Gaussian (LG) distributions yields an excellent result:

$$D_{\text{test}}(E) = \sum_{i=1}^{L}D_i(E) = \sum_{i=1}^{L}\frac{\omega_i}{\sqrt{2\pi}W_i}\exp\left[-\left(\frac{E-V_i}{\sqrt{2}W_i}\right)^2\right]. \tag{15}$$

Where, V_i, W_i, and ω_i are the centroids, the standard deviations, and the weights of the ith Gaussian functions, respectively, with a condition $\sum\omega_i = 1$. L is the number of Gaussians used in the $D_{\text{test}}(E)$ function. With this assumption, the cross sections are given by an analytic function (see also Ref. [19]):

$$\sigma(E)E = \pi R_0^2\sum_{i=1}^{L}\frac{\omega_i W_i}{\sqrt{2\pi}}\left[\sqrt{\pi}Z_i\,\text{erfc}(-Z_i) + \exp\left(-Z_i^2\right)\right], \tag{16}$$

with $Z_i = (E - V_i)/\sqrt{2}W_i$.

It should be mentioned that Eq. (7) is just the same as Eq. (16) with $L = 1$. In an earlier publication (Ref. [19]) where Eq. (7) was discussed, only Refs. [14,15] were cited, and the reciprocal method was not mentioned. This was just for simplicity and because the results for 1G ($L = 1$) reproduce the excitation functions already quite well.

The superior performance of this new cross section formula, Eq. (16), will be described in detail in the next section. Here we want to point out that the reciprocal method can be applied to other representations, e.g.,

$$C_{\text{test}}(E) = \frac{d(\sigma E)}{dE} = \pi R_0^2 T_{\text{test}}(E), \quad \text{with} \int T_{\text{test}}(E)dE = 1, \tag{17}$$

and one can obtain another new cross section formula:

$$\sigma(E)E = \int_{E_0}^{E}\frac{d(\sigma E')}{dE'}dE' = \pi R_0^2\int_{E_0}^{E}T_{\text{test}}(E')dE'. \tag{18}$$

Here, R_0 again is a normalization constant for function $T_{\text{test}}(E)$. The lower integration limits in Eq. (18) are either $E_0 = -Q$ or 0, depending on whether the fusion Q value is negative or positive, respectively. $T_{\text{test}}(E)$ can also be any reasonable function with adjustable parameters. It is well known that $T_{\text{test}}(E)$ is related to the transmission coefficient (see Refs. [3], [7], and [26]).

Equations (14) and (18) are equivalent under the condition

$$B_{\text{test}}(E) = \frac{dT_{\text{test}}(E)}{dE}. \tag{19}$$

But one may start either from an assumed $B_{\text{test}}(E)$ or from an assumed $T_{\text{test}}(E)$ to develop a cross section formula. Because of the different "structures" emphasized in the different representations, the two independent approaches serve as starting points for different studies.

III. IMPROVED STUDY OF BARRIER HEIGHT DISTRIBUTION

By inspection of the $B(E)$ [for brevity, from now on we use $B(E)$ instead of $B_{\text{test}}(E)$] for a large number of systems,

TABLE I. Results of least-squares 3G fits, $\omega_i R^2$, V_i, and W_i (i = 1–3) for 16 fusion excitation functions. N are the numbers of data points of the excitation functions used in the fit.

System	Data range (mb)	N	χ_0^2(3G)	χ_0^2(2G)	χ_0^2(1G)	R (fm)	ω_1R^2 (fm^2)	V_1 (MeV)	W_1 (MeV)	ω_2R^2 (fm^2)	V_2 (MeV)	W_2 (MeV)	ω_3R^2 (fm^2)	V_3 (MeV)	W_3 (MeV)	Ref.
^{16}O + ^{208}Pb	0.000016–1133	38	10.8	12.0	98.0	10.8	13.7	71.78	0.983	94.3	74.06	1.66	8.80	78.09	0.112	[27]
^{32}S + ^{89}Y	0.06–468	23	0.431	0.605	12.6	10.0	39.8	75.44	1.22	53.0	78.39	1.69	8.00	82.68	0.129	[28]
^{40}Ca + ^{40}Ca	0.02–531	21	1.35	1.43	4.48	9.97	36.4	52.58	0.344	58.1	53.27	1.40	4.98	56.70	0.240	[29]
^{40}Ca + ^{96}Zr	0.0027–474	62	1.00	1.09	5.40	9.72	63.8	92.84	2.46	19.3	96.41	1.06	11.25	98.74	0.170	[30]
^{58}Ni + ^{60}Ni	0.04–365	33	2.97	3.23	23.3	8.62	6.98	93.34	0.737	58.7	98.49	2.44	8.66	104.11	0.391	[31]
^{40}Ca + ^{194}Pt	0.061–398	31	11.0	37.5	41.9	10.4	40.09	168.09	3.62	42.9	172.27	0.862	26.0	182.48	0.536	[32]
^{16}O + ^{144}Sm	0.15–876	27	3.19	3.30	21.8	10.6	44.9	59.57	1.11	48.7	60.70	1.41	19.5	64.49	0.240	[33]
^{48}Ca + ^{48}Ca	0.00058–506	27	3.49	4.75	6.60	10.5	72.5	50.90	0.909	21.5	51.93	1.51	15.6	55.66	0.149	[34]
^{40}Ca + ^{90}Zr	0.84–407	40	2.40	2.52	5.33	10.1	61.1	95.44	1.32	16.9	96.02	0.526	24.0	98.68	0.409	[35]
^{11}Be + ^{209}Bi	10.8–889	15	1.31	1.34	1.52	11.6	54.2	36.80	1.51	28.0	39.22	0.519	52.9	43.69	0.304	[36]
^{40}Ca + ^{132}Sn	3.6–541	15	0.975	0.985	1.28	10.9	52.0	113.28	4.11	38.2	115.56	0.962	28.9	116.87	1.88	[37]
^{58}Ni + ^{58}Ni	0.049–226	17	0.486	0.501	4.16	10.5	11.4	94.62	0.790	61.0	99.47	1.98	37.8	108.05	1.37	[38]
^{12}C + ^{30}Si	0.0027–815	22	0.480	0.726	0.934	8.68	22.0	12.82	0.482	22.8	12.82	0.895	30.5	15.96	0.288	[39]
^{24}Mg + ^{30}Si	0.0080–332	20	0.256	0.256	0.499	8.52	23.4	23.44	0.723	46.6	24.60	1.28	2.57	27.48	0.089	[40]
^{40}Ar + ^{112}Sn	0.0085–478	15	0.604	0.613	3.33	9.53	26.1	101.93	1.75	55.8	105.92	2.14	9.06	108.10	1.43	[41]
^{64}Ni + ^{124}Sn	0.0008–126	12	0.076	0.147	0.814	10.1	30.4	152.03	2.07	46.2	158.42	0.598	26.3	165.97	0.577	[42]

we found that there are, fundamentally, two classes of barrier distributions that reproduce very well the two classes of fusion excitation functions, respectively: (1) a 3G multipeak structure and (2) a 4G multipeak structure.

The results of a 3G description for the fusion barrier of nine systems are summarized in the top part of Table I: ^{16}O + ^{208}Pb [27], ^{32}S + ^{89}Y [28], ^{40}Ca + ^{40}Ca [29], ^{40}Ca + ^{96}Zr [30], ^{58}Ni + ^{60}Ni [31], ^{40}Ca + ^{194}Pt [32]. ^{16}O + ^{144}Sm [33], ^{48}Ca + ^{48}Ca [34], and ^{40}Ca + ^{90}Zr [35]. Two examples with a 4G description of the fusion barrier are summarized in the top part of Table II for systems ^{40}Ca + ^{192}Os [32] and ^{16}O + ^{154}Sm [33]. Since these 11 systems were all measured after Rowley's paper [13], barrier distributions extracted from the double-differentiation recipe are available in the literature.

In Tables I and II the χ_0^2 values of different L Gaussian fits (either L = 1–3 or L = 1–4) are included for comparison. Here, χ_0^2 (LG) is defined as

$$\chi_0^2 = \frac{1}{N}\sum_{i=1}^{N}[(\sigma_i - \sigma_{\text{exp-}i})/\Delta\sigma_{\text{exp-}i}]^2, \tag{20}$$

σ_i and $\sigma_{\text{exp-}i}$ are calculated and experimental cross sections, $\Delta\sigma_{\text{exp-}i}$ are the experimental uncertainties, and N is the number of experimental data points [43]. The experimental uncertainties of the cross sections used in the fitting procedure were taken from the original papers. Since these uncertainties are treated differently in the various experiments, the absolute values of χ_0^2 for the different systems are not critical. As can be seen from Tables I and II, for most systems there is a large improvement of χ_0^2 in going from a 1G to a 2G description, while the improvement in going from 2G to 3G or from 3G to 4G is smaller, but the $B(E)$ spectrum changes a lot. The reason for that will be discussed later. Test calculations have been performed where a single cross section was changed by ±20%. The barrier distribution from the 3G (or 4G) fit was practically unchanged, but a substantial change of the barrier distributions obtained from the double-differentiation recipe was observed near these energies.

These two classes of structure will be discussed in detail separately below.

A. 3G description

The barrier distributions $B(E)$ for two systems, ^{40}Ca + ^{194}Pt and ^{16}O + ^{144}Sm, are shown in Figs. 1 and

TABLE II. Results of least-squares 3G and 4G fits, respectively, $\omega_i R^2$, V_i, and W_i (i = 1–3 or 4) for three fusion excitation functions. N are the numbers of data points of the excitation functions used in the fit. The systems are ^{16}O + ^{154}Sm, ^{40}Ca + ^{192}Os, and ^{40}Ar + ^{154}Sm, the data range, data points N, and references are 0.18–33, 37, [33], 0.074–1052,45, [32], and 0.0016–407, 15, [41], respectively.

System	χ_0^2(4G)	χ_0^2(3G)	χ_0^2(2G)	χ_0^2(1G)	R (fm)	ω_1R^2 (fm^2)	V_1 (MeV)	W_1 (MeV)	ω_2R^2 (fm^2)	V_2 (MeV)	W_2 (MeV)	ω_3R^2 (fm^2)	V_3 (MeV)	W_3 (MeV)	ω_4R^2 (fm^2)	V_4 (MeV)	W_4 (MeV)
^{16}O + ^{154}Sm		2.94	2.96	13.0	10.4	14.1	55.13	1.42	40.9	58.92	2.10	53.5	60.38	1.83			
	2.54				10.4	13.1	54.80	1.28	57.8	58.56	1.53	29.7	61.02	0.481	7.18	63.40	0.200
^{40}Ca + ^{192}Os		14.8	15.3	16.7	10.5	53.5	164.79	4.42	33.7	168.15	5.21	23.7	171.33	4.54			
	13.8				10.5	49.5	164.33	4.15	30.6	166.89	4.93	21.0	170.01	0.482	9.59	176.40	0.443
^{40}Ar + ^{154}Sm		0.388	1.44	19.5	11.7	3.35	114.57	2.17	39.8	122.01	3.33	92.9	131.37	3.19			
	0.387				11.7	3.40	114.59	2.18	40.0	122.02	3.32	86.2	131.03	2.95	6.36	136.12	0.364

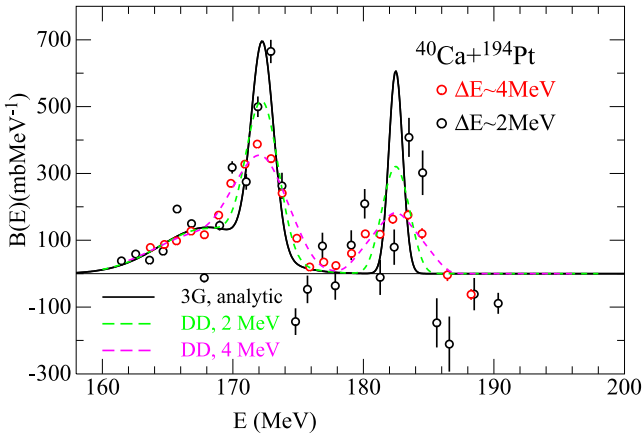

FIG. 1. $B(E)$ spectrum for the system $^{40}\mathrm{Ca}+{}^{194}\mathrm{Pt}$. Curves are obtained by using a 3G description for all or subsets of the measured cross sections.

2, respectively. The open circles in Figs. 1 and 2 show the barrier distributions obtained with the double-differentiation recipe. Each $B(E)$ symbol is calculated from three cross sections (three-point method), which are separated in energy by ΔE. The different colors (red and black) of symbols are obtained with different ΔE. As discussed in Ref. [5], larger values of ΔE are often used in the literature for the double-differentiation recipe, in order to reduce the uncertainty of results. This, however, leads to a damping of the structure in the barrier distribution, as can be seen from a comparison of the black ($\Delta E \approx 1$ or 2 MeV) and red ($\Delta E \approx 2$ or 4 MeV) symbols in Figs. 2 or 1, respectively. The solid-black line in these figures are the results of a 3G description using least-squares fits to the measured excitation functions with Eq. (16), which is obtained with small energy steps (<0.1 MeV) and denoted as "analytic." In order to demonstrate the step-size dependence behavior (ambiguity problem) we have applied the differentiation recipe to the 3G fit curve also. In Fig. 1, the magenta and green long-dashed curves are results determined by applying

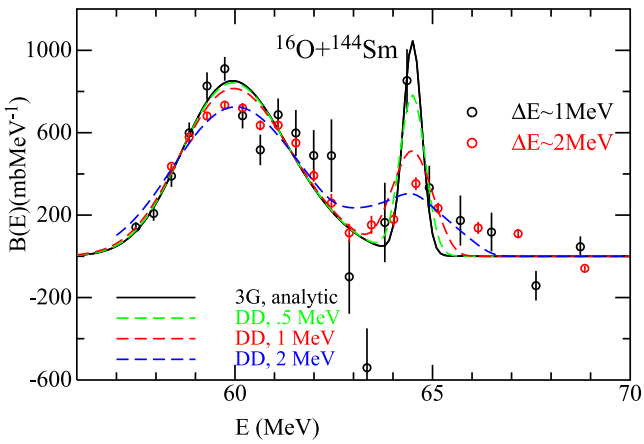

FIG. 2. $B(E)$ spectrum for the system $^{16}\mathrm{O}+{}^{144}\mathrm{Sm}$. Curves are obtained by using a 3G description for all or subsets of the measured cross sections.

TABLE III. Comparison of the χ_0^2 and χ^2 values in the LG fittings for fusion systems $^{16}\mathrm{O}+{}^{144}\mathrm{Sm}$, $^{40}\mathrm{Ca}+{}^{194}\mathrm{Pt}$, $^{16}\mathrm{O}+{}^{154}\mathrm{Sm}$, and $^{40}\mathrm{Ca}+{}^{192}\mathrm{Os}$.

System	LG, M	χ_0^2	χ^2	System	LG, M	χ_0^2	χ^2
$^{40}\mathrm{Ca}+{}^{194}\mathrm{Pt}$	1G, 3	41.9	46.4	$^{16}\mathrm{O}+{}^{144}\mathrm{Sm}$	1G, 3	21.8	24.5
$N=31$	2G, 6	37.5	46.5	$N=27$	2G, 6	3.3	4.3
	3G, 9	11.0	15.5		3G, 9	3.2	4.8
$^{16}\mathrm{O}+{}^{154}\mathrm{Sm}$	1G, 3	13.0	14.1	$^{40}\mathrm{Ca}+{}^{192}\mathrm{Os}$	1G, 3	16.7	17.9
$N=37$	2G, 6	3.0	3.5	$N=45$	2G, 6	15.3	17.7
	3G, 9	2.9	3.9		3G, 9	14.8	18.5
	4G, 12	2.5	3.7		4G, 12	13.8	18.2

the double-differentiation recipe on the black curve, with $\Delta E = 4$ or 2 MeV, respectively. The magenta line in Fig. 1 reproduces the red circle results [determined by applying the double-differentiation (DD) recipe to the experimental cross sections with $\Delta E \approx 4$ MeV] very well for all three peaks. The black circles, derived with $\Delta E \approx 2$ MeV, show a large scatter including some negative points; however, the green curve reproduces the average behavior very well.

For the $^{40}\mathrm{Ca}+{}^{194}\mathrm{Pt}$ system, the value of χ_0^2 from 1G to 2G and 3G improves from 41.9 to 37.5 and 11.0, successively. In this case, the third ($i=3$) peak in the 3G description nearly, but not exactly, agrees with the results obtained from any of the double-differentiation recipes ($\Delta E = 2$ or 4 MeV). This is because the fit was made to the measured fusion cross sections and not to the points obtained from the double-differentiation recipe, which have the disadvantage of step-size (ΔE) dependence.

There are two kinds of systems in Table I. For the systems given in the upper six rows, a 2G description does not reproduce the narrow peak at high energy. One must use a 3G description to obtain a detailed $B(E)$ spectrum. For three of the systems in the middle part of the Table I the 2G description already gives the narrow high energy peak, and the low energy peak splits into two bumps in the 3G description. It follows that for these cases a 2G description is already a rather good description. Obviously this behavior is related to the ratios of strength between the three components.

One may ask, for system $^{16}\mathrm{O}+{}^{144}\mathrm{Sm}$ or $^{40}\mathrm{Ca}+{}^{194}\mathrm{Pt}$, while a 3G fit is good, what happens for a 4G fit? In principle, a fit by using a formula with more adjustable parameters often leads to a smaller χ_0^2 value. But there is another χ^2 value that should be considered, which includes the idea of degrees of freedom:

$$\chi^2 = \frac{N}{N-M}\chi_0^2. \tag{21}$$

Here, N is the number of fusion data points used in the fit as indicated above, and M is the number of parameters used in the formula. For 1G to 5G, M are 3, 6, 9, 12, and 15, respectively. In principle, while L increases, a smaller χ_0^2 in the least-squares fit is obtained. But, it is a meaningful improvement only if a smaller χ^2 value is obtained at the same time. In Table III, values of χ^2 and χ_0^2 for systems, $^{16}\mathrm{O}+{}^{144}\mathrm{Sm}$, $^{40}\mathrm{Ca}+{}^{194}\mathrm{Pt}$, $^{16}\mathrm{O}+{}^{154}\mathrm{Sm}$, and $^{40}\mathrm{Ca}+{}^{192}\mathrm{Os}$ are compared. For the $^{16}\mathrm{O}+{}^{144}\mathrm{Sm}$ and $^{40}\mathrm{Ca}+{}^{194}\mathrm{Pt}$ systems, χ^2 increases

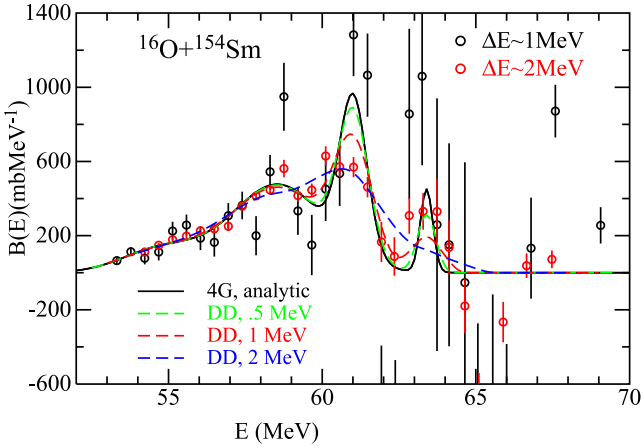

FIG. 3. $B(E)$ spectrum for the system $^{16}\mathrm{O}+^{154}\mathrm{Sm}$. Curves are obtained by using a 4G description for all or subsets of the measured cross sections.

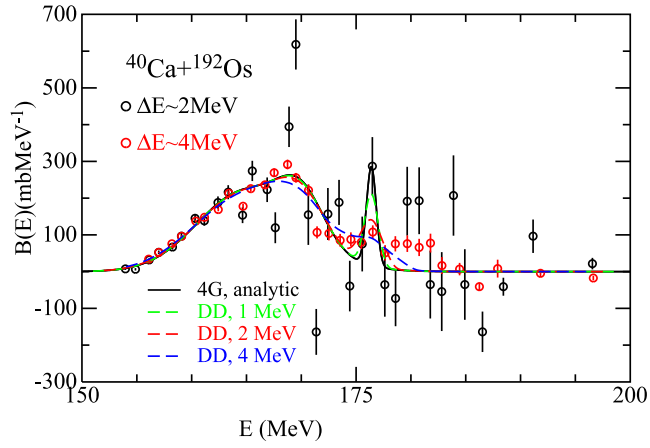

FIG. 4. $B(E)$ spectrum for the system $^{40}\mathrm{Ca}+^{192}\mathrm{Os}$. Curves are obtained by using a 4G description for all or subsets of the measured cross sections.

substantially for 4G ($M = 12$), thus offering no acceptable improvement. Thus, for $^{40}\mathrm{Ca}+^{194}\mathrm{Pt}$, 3G is undoubtedly the best. For $^{16}\mathrm{O}+^{144}\mathrm{Sm}$, 2G and 3G are similar and both are acceptable (for 3G, $\chi^2 = 4.8$, only little worse than in 2G, 4.3).

For system $^{16}\mathrm{O}+^{144}\mathrm{Sm}$ comparison with previous analyses may be discussed. The CC calculations give a result with a χ_0^2 value of 36.5 [33]. Recently Hagino [44] developed a new method for obtaining the barrier distribution by assuming that the excitation function is a sum of several components, each described by the Wong formula. For system $^{16}\mathrm{O}+^{144}\mathrm{Sm}$, Hagino's result gives a χ_0^2 value of 15.1. Obviously the χ_0^2 value 3.2 obtained from a 3G description is better than these previous results.[2]

B. 4G description

The prime examples for a 4G barrier description are the $^{16}\mathrm{O}+^{154}\mathrm{Sm}$ and $^{40}\mathrm{Ca}+^{192}\mathrm{Pt}$ systems, both of which involve highly deformed nuclei. These are shown in Figs. 3 and 4, respectively.

As mentioned above for systems $^{16}\mathrm{O}+^{144}\mathrm{Sm}$ and $^{40}\mathrm{Ca}+^{194}\mathrm{Pt}$, the χ^2 values increase substantially when changing the barrier description 3G to the 4G. In contrast, for systems $^{16}\mathrm{O}+^{154}\mathrm{Sm}$ and $^{40}\mathrm{Ca}+^{192}\mathrm{Pt}$, the χ^2 values improve when changing the barrier description from 3G to 4G, but get significantly poorer when changing from 4G to 5G. In these two cases, 4G is the best description.

The meanings of symbols and lines in Figs. 3 and 4 are the same as in Figs. 1 and 2, with the only difference being that 4G descriptions are added in Figs. 3 and 4. From these two figures, it is clear that one arrives at the same conclusion as above. That is, a much better description of the barrier height distribution is achieved using the present method when compared with previous results using the double-differentiation recipe. The present result yields a clear spectrum, which is not the case with the previous methods. Further, it displays patterns and features that are "hidden" in the previous attempts using different ΔE.

Both systems $^{16}\mathrm{O}+^{154}\mathrm{Sm}$ and $^{40}\mathrm{Ca}+^{192}\mathrm{Pt}$ are highly deformed, and their $B(E)$ spectra are rather different from those discussed in Sec. III A. Note that, in these cases, the peak at high energy was revealed only with a 4G description. This high energy peak in $B(E)$ was observed in previous analyses with the double-differentiation recipe but is very step-size dependent. For system $^{16}\mathrm{O}+^{154}\mathrm{Sm}$, CC calculations (green) and analyses using five components of the Wong formula conducted by Hagino (magenta) are compared with the 4G results (black) in Fig. 5. The high energy peak was not expected from the CC calculations and appeared as a weak tail in Hagino's analysis. The χ_0^2 values for CC calculations [33], Hagino's new analysis [44], and the 4G description are 13.2, 88.9 and 2.54, respectively. Clearly, the present 4G description is the best.

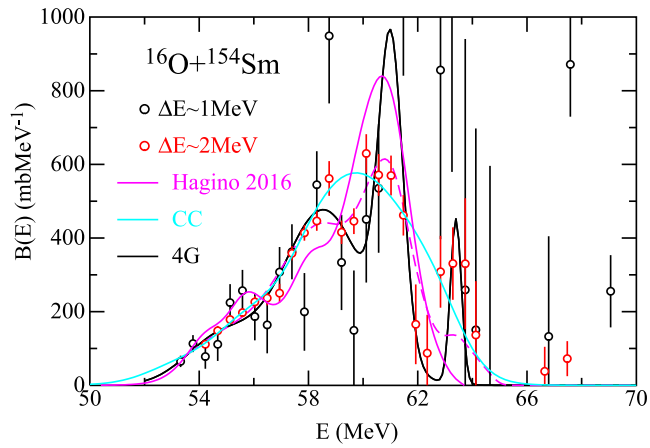

FIG. 5. $B(E)$ spectrum for the system $^{16}\mathrm{O}+^{154}\mathrm{Sm}$. Curves are obtained by using a 4G description, CC, and Hagino's analysis by using five components of the Wong formula.

[2]We do not want to discuss the many papers detailing the different ways of getting a better $B(E)$ spectrum. We refer the reader to, e.g., a recent paper by Scamps [45].

C. Width of the high energy peak of $B(E)$

The FWHM of the high-energy peak obtained in the above two subsections is often about a fraction of a MeV, which is narrower than the peak width obtained in all previous studies with the double-differentiation recipe. The reason for this has been shown: the energy step size used in previous studies is often rather large, thus the peak size is damped if it is a narrow one. It follows that no narrow peak can be well recognized when a smaller energy step, ΔE, is taken, as it would yield huge uncertainties when determined with small energy steps.

In the early days of nuclear reaction studies the heavy-ion fusion excitation functions were explained by the blackbody (strong absorption) model, as given in Eq. (1). The values of the radius, R, and barrier, V, are obtained from the slope and the intersection with the abscissa in a linear plot of $\sigma_b(E)E$ vs E with Eq. (1), which only gives a good description of fusion excitation functions for cross sections larger than ≈100 mb. This formula is based on classical mechanics, neglecting the wave properties of the incident beam [8]. Thus, it should be applied at the energy range above the Coulomb barrier. Rowley obtained the corresponding barrier distribution of Eq. (1), which is a δ function [13]:

$$\frac{1}{\pi R^2}\frac{d^2(\sigma_b(E)E)}{dE^2} = \delta(E - V). \tag{22}$$

The physics picture behind the fusion enhancement at energies around and lower than the Coulomb barrier was first introduced by Dasso *et al.,* [10] and is often cited in the literature. With a qualitative consideration, he showed that the sub-barrier fusion enhancement, which is not reproduced by Eq. (1), can be approximately understood by a splitting of the Coulomb barrier into two barriers due to channel couplings. These two components are located at energies below and above the original Coulomb barrier.

In the paper where Rowley established the idea to obtain the barrier distribution $B(E)$ with the double derivative $d^2(\sigma E)/dE^2$, he estimated the barrier width due to the quantum mechanical penetration, using Wong's formula, to be about $0.56\hbar\omega$ [13], where $\hbar\omega$ is the curvature at the top of the potential barrier in the Wong formula [9]. This result led Rowley *et al.,* to infer another point: that one can obtain the experimental $B(E)$ by the double-differentiation recipe with a larger energy step size without loss of information, Eespecially because in practice, due to the large uncertainty introduced in the numerical calculations in the double-differentiation recipe, one can only use a large energy step to get a well-defined (not too randomly distributed) $B(E)$ at higher energies with the double-differentiation recipe. This guess that larger energy step size prevents loss of information has not been proved.

The estimation of $0.56\hbar\omega$ is for a one-peak barrier distribution which includes the quantum mechanical penetration effect. For a multipeak $B(E)$, influences of the quantum penetration effect on the various components may be different. At peaks whose energy is higher than the Coulomb energy, the quantum mechanical effect is weaker and the strong absorption effect will most likely be dominant.

Naively, Dasso's theory [10] covers the energy region originally described with the black-body model. In reality, it is not so simple. The two (or three) broader peaks in 3G (or 4G) descriptions obtained in Secs. III A and III B are at lower energies. That is what has been described qualitatively by the two components in $B(E)$ in Dasso's theory. Because in that paper Dasso *et al.* focused their study around and lower than the barrier, the cross section range discussed is less than 150 mb.

The narrow peak appears at an energy above the barrier, where the fusion cross sections are above 100 mb and the fusion excitation functions are nearly a straight line in a σE vs E plot. The location of this narrow peak is always at an energy several MeV higher than the value of V determined from Eq. (1), the classical, blackbody model. The two components description in Dasso's theory, devoted to explain fusion enhancement, did not emphasize well fusion for all energy regions. At higher energies (above the Coulomb barrier), rather pure strong absorption behavior takes effect, which may be described with the blackbody model approximately. Of course, quantum mechanical penetration effects are present also, leading to a narrow, but not a delta, peak. This is only a preliminary, tentative discussion; we leave it as an open question, which needs to be studied further.

As pointed out by Bierman *et al.,* [32], the energy separation of the two low-energy components is, on average, proportional to the charge product Z_1Z_2. This energy separation is smaller (≈1 MeV) for the system of $^{16}O + ^{144}Sm$ and therefore easily identified. In this case, the 2G result is already good enough, as detailed above; see Table III. For cases with deformed target nuclei, not two but three or more peaks have to be included in the Dasso consideration.

It is important to mention that, in order to give detailed comparisons of the CC calculations and the 3G or 4G description, and to get an understanding of the narrower component in $B(E)$, the theoretical CC calculations have to be improved in many cases, so that the double differentiation of σE can be taken numerically with an energy step of less than 0.1 MeV.

D. Another advantage for the *L*G description

The data discussed in the previous sections were all measured in small energy steps, which, as mentioned earlier, is a requirement for applying the double-differentiation recipe. In this section we will describe another important advantage of the new method for the analysis of systems which have not been measured in small energy steps. For a comparison we have chosen the systems $^{16}O + ^{144}Sm$ and $^{40}Ca + ^{96}Zr$, for which 27 and 62 data points are available, respectively. Figure 6(a) shows the results of a 3G description, using all, every other, or every third data point for the $^{16}O + ^{144}Sm$ excitation function. Similar results for the system $^{40}Ca + ^{96}Zr$ excitation function, using all or every sixth data point are shown in Fig. 6(b). For both cases, the data at the highest and lowest energy points are always included.

As expected, with the *L*G description method, results from using fewer data points are rather similar to results with all data points. Here the wide range of the measure-

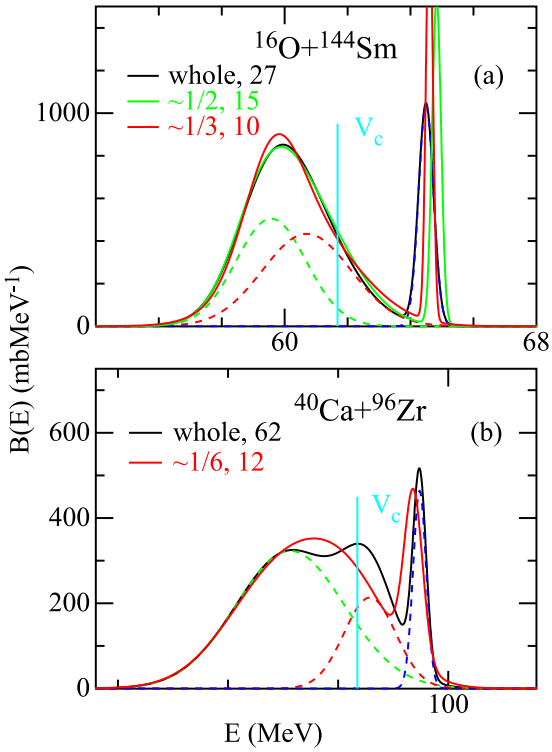

FIG. 6. $B(E)$ spectra for the systems $^{16}O + ^{144}Sm$ [33] (a) and $^{40}Ca + ^{96}Zr$ [30] (b). Solid curves are fittings with a 3G description. The black and the colored ones are obtained from the whole dataset or from the subsets of the measured cross sections, respectively. Dashed curves are the three corresponding components for the whole dataset.

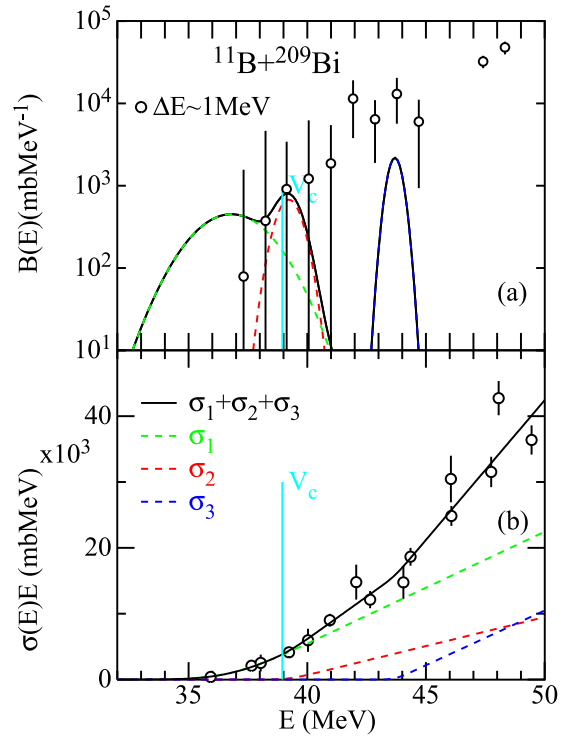

FIG. 7. Spectra for the system $^{11}Be + ^{209}Bi$ [36]: excitation function (b) and barrier distribution (a). The solid curves are obtained from least-squares fits to the measured cross sections using a 3G description. Dashed curves are the three corresponding components.

ment is important. The ability to determine a fusion barrier distribution with only 10 or 12 data points for systems $^{16}O + ^{144}Sm$ or $^{40}Ca + ^{96}Zr$, respectively, is a clear advantage of this method for reactions with radioactive beams which are usually measured only with large energy steps. The present method can also be applied to fusion studies in lighter systems.

Results from seven experiments and one other experiment, which were not measured with small energy steps, are listed in the third part of Table I and the second part of Table II, respectively. These include two systems from radioactive beam experiments: $^{11}Be + ^{209}Bi$ [36] and $^{40}Ca + ^{132}Sn$ [37]. The excitation function and the barrier distribution obtained from a 3G least-squares fit for the system $^{11}Be + ^{209}Bi$ are shown in Fig. 7. Obviously, in this case, results of $B(E)$ obtained with the double-differentiation recipe are not practical to study the reaction dynamics. However, three components can still be obtained in the analysis with a 3G description. It is interesting to note that the barrier distribution for $^{11}Be + ^{209}Bi$ (Fig. 7) resembles the one from the system $^{16}O + ^{208}Pb$, which also involves a closed n-shell nucleus.

Note that the hindrance phenomenon is well reproduced with a multi-Gaussian fit (as also discussed in Ref. [19]). For fusion of $^{11}Be + ^{209}Bi$, an S-factor maximum is predicted at around 30 MeV from the 3G fit, near the prediction from systematic studies of the hindrance phenomenon [17,46].

IV. SUMMARY

After a general discussion about the methods to obtain formulas of fusion cross sections, a new method, *the reciprocal of a fusion representation*, was illustrated of extracting a fusion cross section formula and the fusion barrier distribution in heavy ion reactions, namely, based on a double integration of a parametrized barrier distribution $D(E)$: $\sigma(E)E = \pi R^2 \int_{E_0}^{E} (\int_{E_0}^{E'} D(B)dB)dE'$. It was found that either a three-Gaussian (3G) or a four-Gaussian (4G) description of $D(E)$ provides an analytic formula of the fusion excitation function which can reproduce the experimental excitation functions for a large number of systems extremely well across a cross section range covering eight orders of magnitude. This method can also be applied to fusion reactions involving lighter heavy ions and to measurements which have been taken only in larger energy steps, which is important for the study of fusion reactions induced by radioactive projectiles.

The fusion barrier distribution obtained with this method is much improved over those from previous studies using the double-differentiation recipe, which suffers from the ambiguity problem due to the energy-step-size dependence and large uncertainties of the determined results.

It was found that there is a narrow barrier peak at energies higher than the Coulomb barrier for most fusion systems, which, in the past, has not been seen or recognized. The physical meaning and interpretation of this peak, related to

the strong absorption property of the nuclear reaction at higher energies, is an interesting issue, to be studied further.

The improved $B(E)$ spectrum will be beneficial for studies of the reaction dynamics. Its capability of describing the fusion hindrance phenomenon opens new possibilities for studies at low bombarding energies.

ACKNOWLEDGMENTS

This work was supported by the U.S. Department of Energy, Office of Nuclear Physics, under Contract No. DE-AC02-06CH11357. The authors want to thank K. E. Rehm, B. B. Back, K. Hagino, A. M. Stefanini, and G. Montagnoli for many interesting discussions.

[1] V. I. Zagrebaev, A. S. Denikin, A. V. Karpov, A. P. Alekseev, M. A. Naumenko, V. A. Rachkov, and V. V. Samarin, NRV web knowledge base on low-energy nuclear physics, http://nrv.jinr.ru/, accessed in 2020.
[2] M. Dasgupta, D. J. Hinde, N. Rowley, and A. M. Stefanini, Annu. Rev. Nucl. Part. Sci. **48**, 401 (1998).
[3] A. B. Balantekin and N. Takigawa, Rev. Mod. Phys. **70**, 77 (1998).
[4] K. Hagino and N. Takigawa, Prog. Theor. Phys. **128**, 1061 (2012).
[5] B. B. Back, H. Esbensen, C. L. Jiang, and K. E. Rehm, Rev. Mod. Phys. **86**, 317 (2014).
[6] G. Montagnoli and A. M. Stefanini, Eur. Phys. J. A **53**, 169 (2017).
[7] C. L. Jiang, B. B. Back, K. E. Rehm, K. Hagino, G. Montagnoli and A. M. Stefanini, Eur. Phys. J. A **57**, 235 (2021).
[8] J. M. Blatt and V. F. Weisskopf, *Theoretical Nuclear Physics* (John Wiley and Sons, New York, 1952), p. 346.
[9] C. Y. Wong, Phys. Rev. Lett. **31**, 766 (1973).
[10] C. H. Dasso, S. Landowne, and A. Winther, Nucl. Phys. A **405**, 381 (1983).
[11] C. H. Dasso, S. Landowne, and A. Winther, Nucl. Phys. A **407**, 221 (1983).
[12] P. H. Stelson, Phys. Lett. B **205**, 190 (1988); P.H. Stelson, H.J. Kim, M. Beckerman, D. Shapira, R.L. Robinson, Phys. Rev. C **41**, 1584 (1990).
[13] N. Rowley, G. R. Satchler, and P. H. Stelson, Phys. Lett. B **254**, 25 (1991).
[14] K. Siwek-Wilczynska, I. Skwira, and J. Wilczynski, Acta Phys. Pol. B **34**, 1867 (2003).
[15] K. Siwek-Wilczynska and J. Wilczynski, Phys. Rev. C **69**, 024611 (2004).
[16] C.L. Jiang, H. Esbensen, K.E. Rehm, B.B. Back, R.V.F. Janssens, J.A. Caggiano, P. Collon, J. Greene, A.M. Heinz, D.J. Henderson, I. Nishinaka, T.O. Pennington, and D. Seweryniak, Phys. Rev. Lett. **89**, 052701 (2002).
[17] C. L. Jiang *et al.*, Phys. Rev. C **69**, 014604 (2004).
[18] C.L. Jiang, K.E. Rehm, R.V.F. Janssens, H. Esbensen, I. Ahmad, B.B. Back, P. Collon, C.N. Davids, J.P. Greene, D.J. Henderson, G. Mukherjee, R.C. Pardo, M. Paul, T.O. Pennington, D. Seweryniak, S. Sinha, and Z. Zhou, Phys. Rev. Lett. **93**, 012701 (2004).
[19] C. L. Jiang, K. E. Rehm, B. B. Back, A. M. Stefanini, and G. Montagnoli, Eur. Phys. J. A **54**, 218 (2018).
[20] S. Mişicu and H. Esbensen, Phys. Rev. Lett. **96**, 112701 (2006); Phys. Rev. C **75**, 034606 (2007).
[21] T. Ichikawa, K. Hagino, and A. Iwamoto, Phys. Rev. C **75**, 057603 (2007); Phys. Rev. Lett. **103**, 202701 (2009). T. Ichikawa and K. Matsuyanagi, Phys. Rev. C **88**, 011602(R) (2013).
[22] V. Yu. Denisov and I. Yu. Sedykh, Eur. Phys. J. A **55**, 153 (2019).
[23] C. L. Jiang, Eur. Phys. J. A **58**, 72 (2022).
[24] C.L. Jiang, K.E. Rehm, B.B. Back, and R. V. F. Janssens, Phys. Rev. C **75**, 015803 (2007).
[25] H. Esbensen and C. L. Jiang, Phys. Rev. C **79**, 064619 (2009).
[26] H. Esbensen, Phys. Rev. C **85**, 064611 (2012).
[27] M. Dasgupta, D.J. Hinde, A. Diaz-Torres, B. Bouriquet, C.I. Low, G.J. Milburn, and J. O. Newton, Phys. Rev. Lett. **99**, 192701 (2007); C.R. Morton, A.C. Berriman, M. Dasgupta, D.J. Hinde, J.O. Newton, K. Hagino, and I. J. Thompson, Phys. Rev. C **60**, 044608 (1999).
[28] A. Mukherjee, M. Dasgupta, D.J. Hinde, K. Hagino, J.R. Leigh, J.C. Mein, C.R. Morton, J.O. Newton, and H. Timmers, Phys. Rev. C **66**, 034607 (2002)
[29] G. Montagnoli, A.M. Stefanini, C.L. Jiang, H. Esbensen, L. Corradi, S. Courtin, E. Fioretto, A. Goasduff, F. Haas, A.F. Kifle, C. Michelagnoli, D. Montanari, T. Mijatovic, K.E. Rehm, R. Silvestri, P.P. Singh, F. Scarlassara, S. Szilner, X.D. Tang, and C.A. Ur, Phys. Rev. C **85**, 024607 (2012).
[30] A. M. Stefanini *et al.*, Phys. Lett. B **728**, 639 (2014).
[31] A.M. Stefanini, D. Ackermann, L. Corradi, D.R. Napoli, C. Petrache, P. Spolaore, P. Bednarczyk, H.Q. Zhang, S. Beghini, G. Montagnoli, L. Mueller, F. Scarlassara, G.F. Segato, F. Soramel, and N. Rowley, Phys. Rev. Lett. **74**, 864 (1995).
[32] J. D. Bierman *et al.*, Phys. Rev. Lett. **76**, 1587 (1996); Phys. Rev. C **54**, 3068 (1996).
[33] J.R. Leigh, N. Rowley, R.C. Lemmon, D.J. Hinde, J.O. Newton, J.X. Wei, J.C. Mein, C.R. Morton, S. Kuyucak, and A.T. Kruppa, Phys. Rev. C **47**, R437 (1993); **52**, 3151 (1995).
[34] A. M. Stefanini *et al.*, Phys. Lett. B **679**, 95 (2009).
[35] H. Timmers *et al.*, Phys. Lett. B **399**, 35 (1997).
[36] C. Signorini *et al.*, Nucl. Phys. A **735**, 329 (2004).
[37] J. J. Kolata *et al.*, Phys. Rev. C **85**, 054603 (2012).
[38] M. Beckerman, J. Ball, H. Enge, M. Salomaa, A. Sperduto, S. Gazes, A. DiRienzo, and J.D. Molitoris, Phys. Rev. C **23**, 1581 (1981).
[39] W. J. Jordan, J. V. Maher, and J. Peng, Phys. Lett. B **87**, 38 (1979); G. Montagnoli *et al.*, Phys. Rev. C **97**, 024610 (2018).
[40] A. Morsad, J. J. Kolata, R. J. Tighe, X. J. Kong, E. F. Aguilera, and J. J. Vega, Phys. Rev. C **41**, 988 (1990); C.L. Jiang, A.M. Stefanini, H. Esbensen, K.E. Rehm, S. Almaraz-Calderon, B.B. Back, L. Corradi, E. Fioretto, G. Montagnoli, F. Scarlassara, D. Montanari, S. Courtin, D. Bourgin, F. Haas, A. Goasduff, S. Szilner, and T. Mijatovic, Phys. Rev. Lett. **113**, 022701 (2014).
[41] W. Reisdorf *et al.*, Nucl. Phys. A **438**, 212 (1985).

[42] C.L. Jiang, A.M. Stefanini, H. Esbensen, K.E. Rehm, S. Almaraz-Calderon, M.L. Avila, B.B. Back, D. Bourgin, L. Corradi, S. Courtin, E. Fioretto, F. Galtarossa, A. Goasduff, F. Haas, M.M. Mazzocco, D. Montanari, G. Montagnoli, T. Mijatovic, R. Sagaidak, D. Santiago-Gonzalez, F. Scarlassara, E.E. Strano, and S. Szilner, Phys. Rev. C **91**, 044602 (2015).

[43] This definition of χ_0^2 is often used in many theoretical papers, e.g., [44].

[44] K. Hagino, Phys. Rev. C **93**, 061601(R) (2016).

[45] G. Scamps, Phys. Rev. C **97**, 044611 (2018).

[46] C. L. Jiang, B. B. Back, H. Esbensen, R. V. F. Janssens, and K. E. Rehm, Phys. Rev. C **73**, 014613 (2006).